



Microwave Assisted Synthesis of MoS₂/PANI/ZnO Nanocomposites as a Working Electrode for Energy Storage Applications

J. BALAVIJAYALAKSHMI* and S. KRITHIKA^{ORCID}

Department of Physics, PSGR Krishnammal College for Women, Coimbatore-641004, India

*Corresponding author: E-mail: balavijayalakshmiroopa@gmail.com

Received: 28 March 2021;

Accepted: 2 May 2021;

Published online: 26 June 2021;

AJC-20401

Transition metal dichalcogenide and polyaniline doped zinc oxide nanocomposites influence the transition probabilities and electronic structure. In present study, the various concentrations of MoS₂/PANI/ZnO nanocomposites are synthesized by microwave assisted method. These nanocomposites are characterized by using XRD, FESEM, HRTEM and FT-IR. The XRD results revealed an average crystallite size of synthesized nanocomposites, which was found to be 19-24 nm. The electrochemical properties of the nanocomposites are studied through the CV, EIS and GCD for the application of supercapacitor as an active electrode material. The MoS₂/PANI/ZnO nanocomposites exhibited a specific capacitance of 577 F g⁻¹ and also retained 90% of its initial specific capacitance even after 5000 cycles. Hence MoS₂/PANI/ZnO nanocomposites have potential application for energy storage applications.

Keywords: Molybdenum disulfide, Zinc oxide, Polyaniline, Energy storage, Electrochemical properties.

INTRODUCTION

Supercapacitors are needed as electrochemical storage devices that have been attracting considerable attention in recent years. Supercapacitors have higher power density, rapid charge and discharge time, long term cyclic stability, good operational safety and eco-friendly materials. These materials store and release energy based on (i) the accumulation of charges at the interface between electrode and electrolyte (EDLC); and (ii) fast and reversible faradic redox reactions (pseudocapacitor) depending on the nature of activated materials [1]. Electrochemical supercapacitors stores energy by using double layer and pseudocapacitance processes. Metal oxides and conducting polymers are widely used for redox supercapacitors. Carbon materials are the main electrode materials used for the double layer capacitors. Transition metal oxides doped on conducting polymers are potential material for the supercapacitor application because of electrochemical behaviour [2]. Transition metal dichalcogenide materials (MoS₂) have large surface area, thin and transparent semiconductor, high electrical conductivity, good chemical stability and mechanical strength and exhibit the unique physical, optical and electrical properties, which makes it interesting for using it in nano electronics and

optoelectronics as an enhanced energy harvester [3]. The MoS₂ nanosheets consists of a metal Mo layer sandwiched between two S layers with these triple layers stacking together to form a layered structure. The layered MoS₂ acts as a better functional material because the 2d-electron correlate among Mo atoms and used in enhancing planar electric transportation properties. MoS₂ is rich in molybdenite and can be exfoliated as layered nanosheets that exhibit the high specific capacitance and better cyclic stability [4].

Conducting polymers is a family of compounds composed of monomers with the conjugated chemical bonds that under doping ensures the electron conductivity of the polymer. Polyaniline (PANI) is the enriching conducting polymers because of its good electrical conductivity, easy and economic fabrication processes, better redox properties and high stability [5]. Hence in present study, an attempt is made to prepare a new type of hybrids like MoS₂/PANI impregnated ZnO electrodes for supercapacitor applications. Among the various transition metal oxides, ZnO have used in various applications such as gas sensor, solar cells, optoelectronic devices, catalytic and energy storage applications. Due to its superior properties, low cost, non-toxicity and high surface activity. ZnO is a potential semiconductor received greatest attention for battery applica-

tions. Hence in present study, an attempt is made to prepare a new type of hybrids like MoS₂/PANI nanosheets impregnated with ZnO nanoparticles for supercapacitor applications. Ren *et al.* [6] have synthesized three-dimensional tubular MoS₂/PANI hybrid electrode to obtain the high-rate supercapacitor with the specific capacitance of 552 F g⁻¹ at current density of 0.5 A g⁻¹. Huang *et al.* [7] have synthesized polyaniline/2D graphene analog MoS₂ composites for high-performance supercapacitor. The composites exhibited the specific capacitance as 575 F g⁻¹ at 1 A g⁻¹. Dhibar *et al.* [8] have synthesized the transition metal-doped polyaniline/single-walled carbon nanotubes nanocomposites to obtain the efficient specific capacitance of 546 F g⁻¹ at current density of 0.5 A g⁻¹.

In this study, molybdenum disulfide doped polyaniline and Zinc oxide are synthesized by using a microwave assisted method. Microwave assisted synthesis is a novel green approach which can reduce the waste materials generation, cost and energy. Thus, it can be represented as the eco-friendly synthesis with low energy consumption rate and scaled up product. MoS₂/PANI/ZnO nanocomposites may be a potential electrode material with high specific capacitance due to the synergistic effect between MoS₂/PANI/ZnO provides a large number of active sites for electrochemical reaction and serves as an ion channel for rapid electrolyte transportation that can accommodate large volume changes and improves the conductivity of the electrode [9]. The surface morphology, elemental composition and electrochemical property of the synthesized nano composites were examined by XRD, FESEM, HR-TEM, FT-IR, EDX and using electrochemical workstations.

EXPERIMENTAL

The chemicals *viz.* sodium molybdate dihydrate (Na₂MoO₄·2H₂O), thioacetamide, zinc chloride, oxalic acid, polyaniline and ammonium per sulphate ((NH₄)₂S₂O₈) were purchased from Sigma-Aldrich, USA and used without any further purification.

Synthesis of MoS₂/PANI/ZnO nanocomposites: The MoS₂/PANI/ZnO nanocomposites were synthesized using novel microwave assisted method. Sodium molybdate and thioacetamide in the ratio of 1:3 were dissolved in 15 mL of distilled water and added 1:1 ratio of aniline and ammonium per sulphate in the above solution and stirred for 30 min. About 0.04 M of zinc chloride solution was dispersed in the above solution. Thus, the resultant mixture solution was exposed at 360 W of microwave irradiation for 10 min at 160 °C. Thus, the obtained precipitate of MoS₂/PANI/ZnO nanocomposites was dried in a vacuum oven for 12 h at 80 °C. The same procedures were repeated for the synthesis of 0.06 M and 0.08 M of MoS₂/PANI/ZnO nanocomposites.

Characterization: The structure of the synthesized nanocomposites was characterized by using X-ray diffraction with CuKα radiation. The functional group of the synthesized nanocomposites were confirmed using Fourier Transform Infrared Spectroscopy (FT-IR) with a spectral range of 4000-400 cm⁻¹. The surface morphology of the samples was analyzed using field emission scanning electron microscopy and high-resolution transmission electron microscopy. The CV, EIS and GCD

analysis were conducted by using biologic SP-150 electrochemical workstation.

RESULTS AND DISCUSSION

The FT-IR spectra of the prepared MoS₂/PANI/ZnO nanocomposites are shown in Fig. 1. Fig. 1a shows the observed band at 927 cm⁻¹ corresponds to the Mo=S functional group and further the existence of the polyaniline in emeraldine state is confirmed by band at 1622 cm⁻¹ which is associated with C=N stretching mode of quinonoid rings. It is observed from Fig. 1b-d that the band at 1310 cm⁻¹ is due to the formation of Zn-O functional group and further the band at 896 cm⁻¹ corresponds to the vibrational frequency due to the ZnO lattice. The strong absorption band at 3375 cm⁻¹ describes the O-H stretching vibrations of H₂O due to the absorption of moisture [10]. The band at 1113 cm⁻¹ corresponds to the C-N stretching vibration of secondary amine. The diffraction bands that exist in the MoS₂/PANI are also evidenced in MoS₂/PANI/ZnO nanocomposites thereby confirms the composite formation. It is also observed from the FT-IR spectra that the stretching bands are shifted towards lower wave number with the increase in the concentration of zinc chloride from 0.04 M to 0.08 M and this may be due to the aniline monomer that gets adsorbed on the oxide particles, which further confirms the strong adhesion of the MoS₂/PANI nanocomposites with the ZnO nanoparticles [11].

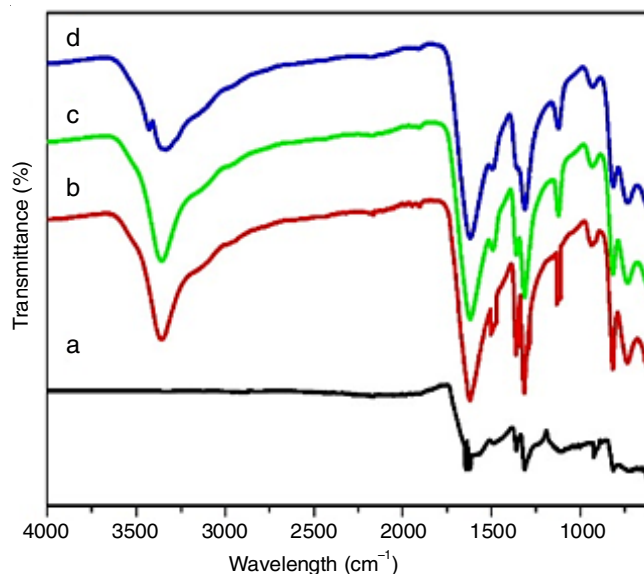


Fig. 1. FT-IR Spectral analysis of (a) MoS₂/PANI nanocomposites, MoS₂/PANI/ZnO nanocomposites using (b) 0.04 M (c) 0.06 M and (d) 0.08 M concentration of zinc chloride

XRD analysis: Fig. 2a-d shows the XRD pattern of MoS₂/PANI and MoS₂/PANI/ZnO (0.04 M, 0.06 M and 0.08 M) nanocomposites. Fig. 2a shows the diffraction peak at 14.27°, 29.8°, 33.65° and 35.39°, which corresponds to the *hkl* planes (002), (004), (101) and (102) respectively, which are well indexed with reference to the JCPDS card No. 37-1492 [12]. The small additional peaks at 20.25° and 25.04° which correspond to the (020) and (200) planes are due to the emeraldine state of poly-

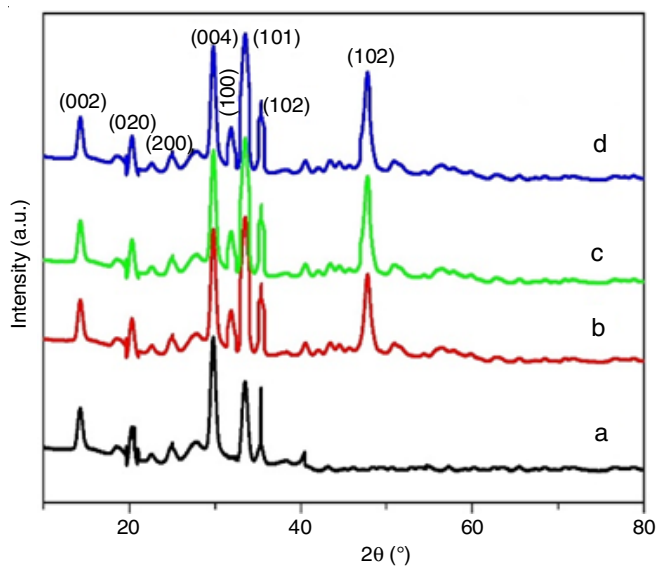


Fig. 2. XRD spectra of (a) MoS₂/PANI nanocomposites and MoS₂/PANI/ZnO nanocomposites using (b) 0.04 M (c) 0.06 M and (d) 0.08M concentration of zinc chloride

aniline and thus confirms the successful formation of MoS₂/PANI nanocomposites. Fig. 2b-d exhibits the peaks at 2θ values

of 14.27°, 29.8°, 33.65°, 35.39°, 20.25°, 25.04°, 31.72° and 47.80° that corresponds to the (002), (004), (101), (102), (020), (200), (100) and (102) planes of MoS₂/PANI and ZnO, respectively which confirms the formation of MoS₂/PANI/ZnO nanocomposites. The intensity of the diffraction peak corresponding to ZnO nanoparticles increases with increase in the concentration of zinc chloride from 0.04 M to 0.08 M and the crystallite size are found to be 19 nm, 22 nm and 24 nm for the various concentrations of 0.04 M, 0.06 M and 0.08M of ZnO nanoparticles, respectively. The crystallite size of the ZnO nanoparticles existed on the MoS₂/PANI nanocomposites is found to be increased for the concentration of 0.08 M of ZnCl₂ and this might be due to the formation of hydrogen bonding between H-N and oxygen of ZnO [13,14]. The presence of no other impurity peaks observed in the XRD analysis and could also be evidenced from EDAX analysis.

FE-SEM analysis: The surface morphology and shape of the synthesized nanocomposites were analyzed by FESEM analysis. Fig. 3a-d exhibits the FESEM images of the prepared MoS₂/PANI and MoS₂/PANI/ZnO (0.04 M, 0.06 M and 0.08 M) nanocomposites. It is observed that the prepared MoS₂/PANI nanocomposites seemed as a sheet like structure, which could also be evidenced from HR-TEM analysis. Fig. 3b-d show that

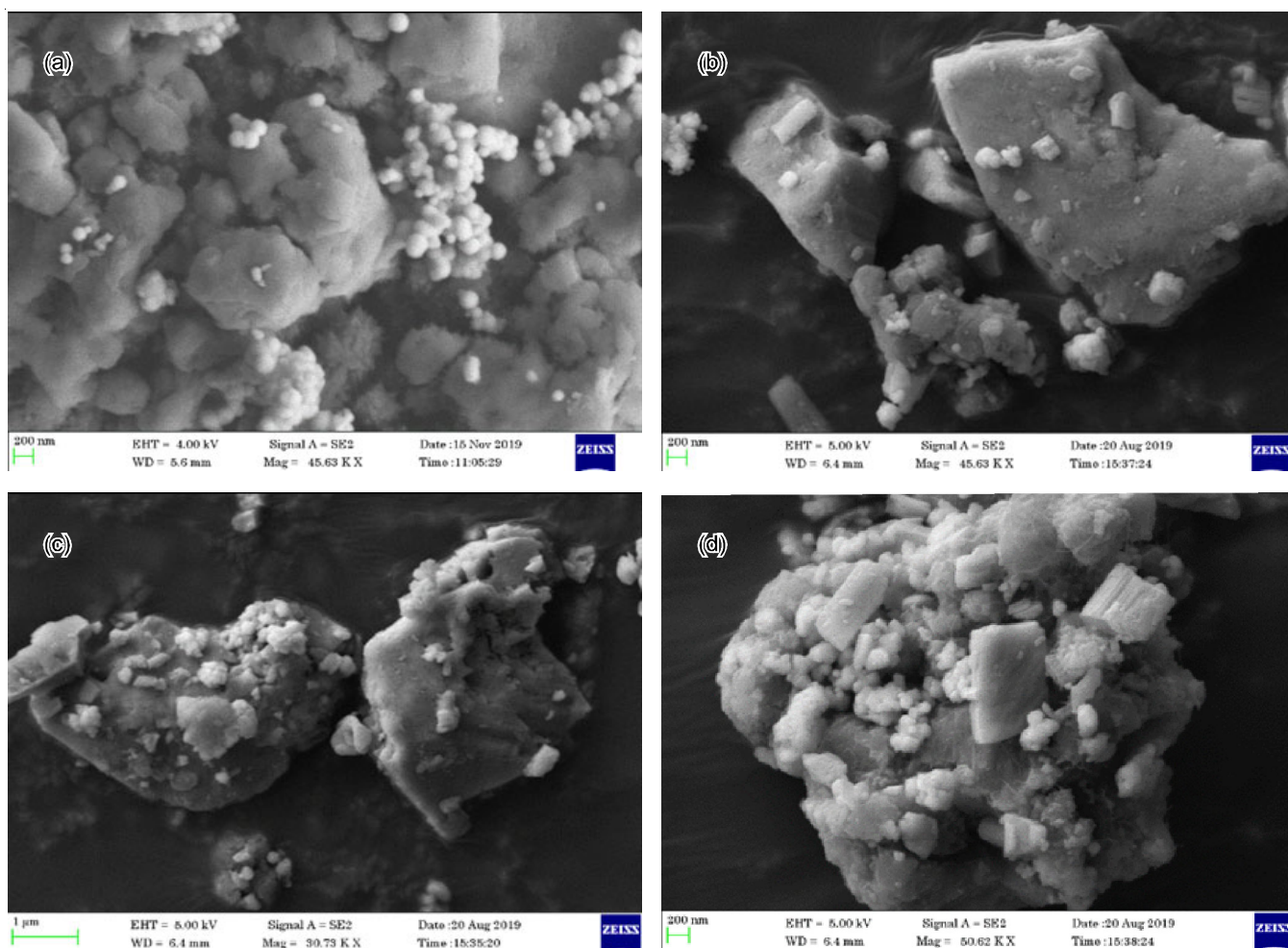


Fig. 3. FESEM images of (a) MoS₂/PANI nanocomposites, MoS₂/PANI/ZnO nanocomposites using (b) 0.04 M (c) 0.06 M and (d) 0.08 M concentration of zinc chloride

the FE-SEM images of different concentrations (0.04 M, 0.06 M, 0.08M) of ZnCl_2 nanoparticles stacked with the MoS_2/PANI nanocomposites. It is observed that the FE-SEM images of $\text{MoS}_2/\text{PANI}/\text{ZnO}$ nanocomposites consists of MoS_2/PANI nanosheets with the rod shape structure of ZnO nanoparticles spread over it and indicates the strong polar interaction between the MoS_2 doped polyaniline and ZnO nanoparticles [15]. It is further observed that as the concentration of zinc oxide increases, the grain size increases, which shows that ZnO starts penetrating into the structure of the MoS_2/PANI nanocomposites.

HR-TEM analysis: Fig. 4a-e show the HR-TEM images of MoS_2/PANI and $\text{MoS}_2/\text{PANI}/\text{ZnO}$ (0.08 M) nanocomposites. Fig. 4a depicts that the synthesized MoS_2/PANI nano-

sheets are thin, spherical and transparent, which may be due to the impact of PANI. It is also observed that the black spots on the surface of MoS_2/PANI nanosheets confirms the formation of well distributed zinc oxide nanoparticles on the surface of MoS_2/PANI nanosheets, which is also evidenced by the FE-SEM analysis. The distributions of ZnO nanoparticles are homogeneous without aggregation, which may be due to the impact of PANI. Hence, from the HR-TEM analysis, the successful synthesis of $\text{MoS}_2/\text{PANI}/\text{ZnO}$ nanocomposite using 0.08 M concentration of zinc chloride is confirmed.

SAED analysis: The selected area electron diffraction pattern (SAED) of the synthesized $\text{MoS}_2/\text{PANI}/\text{ZnO}$ nanocomposites using 0.08 M concentration of ZnCl_2 is shown in Fig. 5.

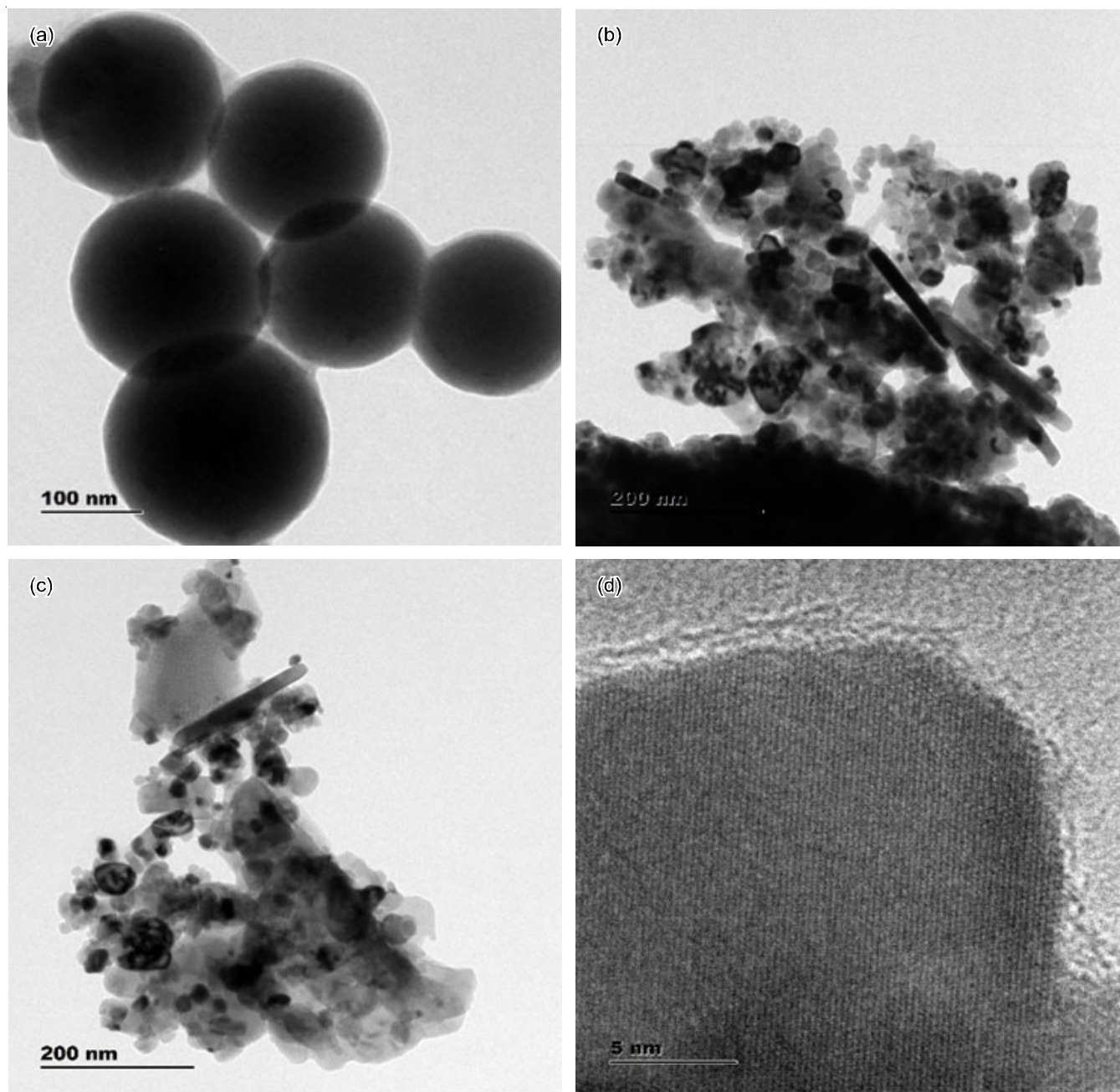


Fig. 4. HRTEM images of (a) MoS_2/PANI nanocomposites (b-d) $\text{MoS}_2/\text{PANI}/\text{ZnO}$ nanocomposites using 0.08 M concentration of zinc chloride

It is observed that there are five discrete bright rings (Fig. 5), which demonstrates the successful decoration of well crystalline face centred cubic of structure zinc nanoparticles on the surface of MoS₂ nanosheets. Each ring observed in the SAED patterns corresponds to the (002), (020), (004), (100) and (102) diffraction planes of MoS₂ and ZnO nanoparticles, which could also be evidenced from XRD analysis.

EDAX analysis: The EDAX spectra of MoS₂/PANI and MoS₂/PANI/ZnO (0.04 M, 0.06 M and 0.08 M) nanocomposites are shown in Fig. 6a-d. Fig. 6a shows the EDAX spectrum of MoS₂/PANI nanocomposites that shows the presence of Mo, S and carbon along with the nitrogen confirms the synthesis of MoS₂/PANI nanocomposites. The EDAX spectra of synthesized MoS₂/PANI/ZnO nanocomposites of various concentrations 0.04 M, 0.06 M, 0.08 M of ZnCl₂ are shown in Fig. 6b-d, which confirms the presence of C, N, Mo, S, Zn and O. It is further confirmed from the EDAX analysis that with increase in the concentration of ZnCl₂ from 0.04 M to 0.08 M, the percentage of zinc and oxygen on the MoS₂/PANI nanocomposites surface increases, which could also be evidenced from FESEM analysis.

Electrochemical properties: The synthesized MoS₂/PANI/ZnO nanocomposites is used as working electrodes materials

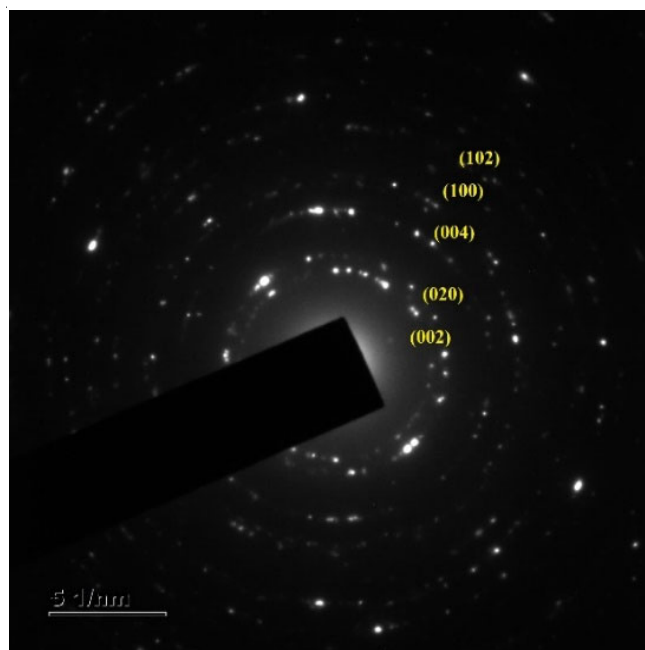


Fig. 5. SAED analysis of MoS₂/PANI/ZnO nanocomposites using 0.08 M concentration of zinc chloride

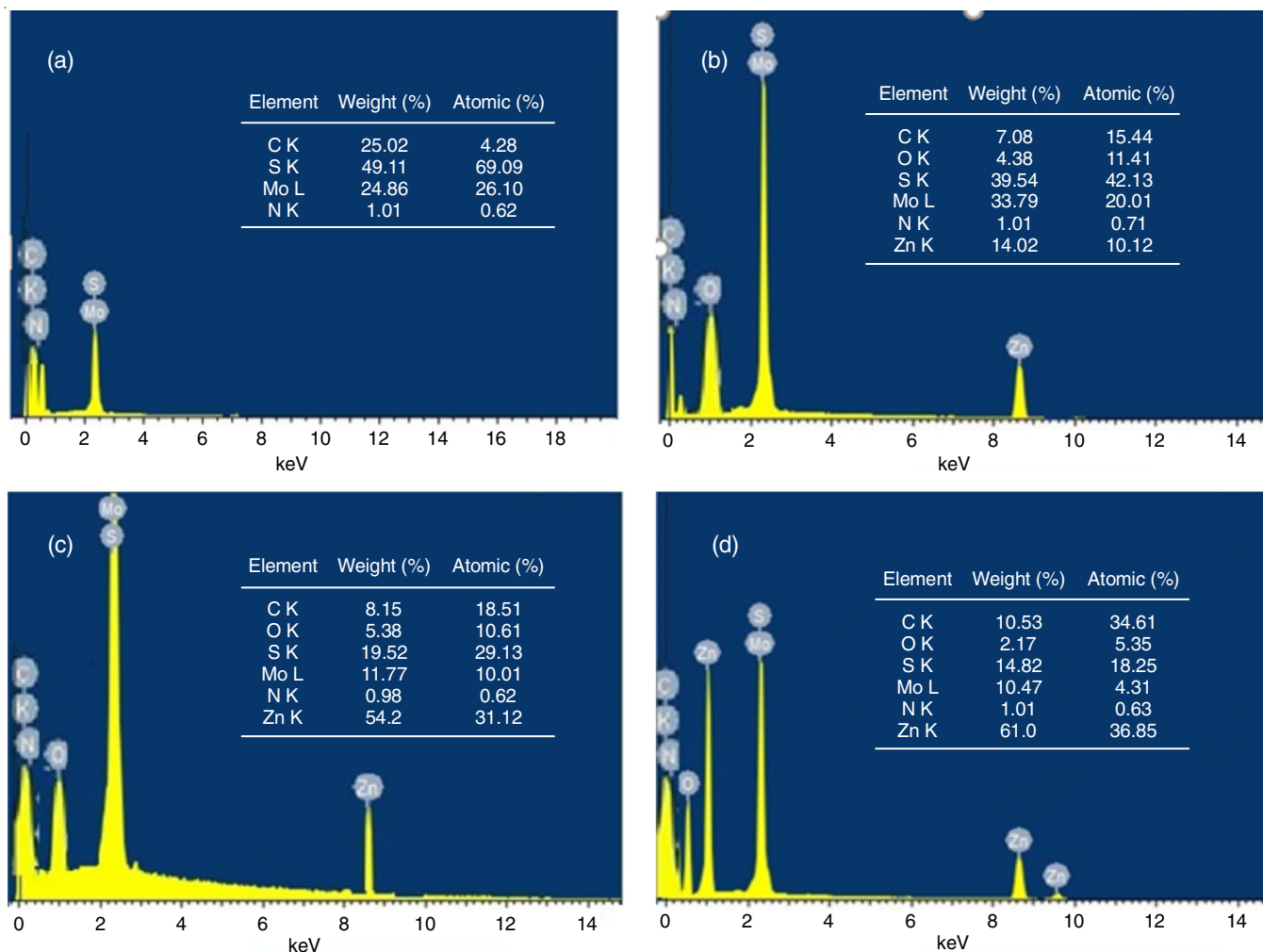


Fig. 6. EDAX analysis of (a) MoS₂/PANI nanocomposites MoS₂/PANI/ZnO nanocomposites using (b) 0.04 M (c) 0.06 M and (d) 0.08 M concentration of zinc chloride

for supercapacitor and are characterized by CV, GCD, EIS and cyclic stability tests in three electrode cell configurations.

Working electrode preparation: The working electrode was prepared by MoS₂/PANI/ZnO nanocomposites, carbon black, polyvinyl difluoride in the ratio of 80:10:10 and mixed together in slurry form. Then the slurry was coated on the nickel foil sheet (1 cm × 1 cm) and dried at 80 °C in 2 h and a solution containing 3 M KOH was used as the electrolyte. The electrochemical behaviour of MoS₂/PANI/ZnO electrode was examined by cyclic voltammetry, galvanostatic charge-discharge and electron impedance spectroscopy analyses using biologic SP-150 electrochemical workstation. The electrochemical analysis was carried out at a room temperature using a three-electrode system in which the electroactive materials platinum foil and Ag/AgCl were used as working counter and reference electrodes, respectively. The CV curves were measured in the potential range of 0 to 0.5 V under the various scan rates from 5 to 100 mV s⁻¹. The EIS measurements were examined in the frequency range from 0.01 Hz to 100 KHz and galvanostatic charge-discharge analyses was performed on the current density of 1-10 mA cm⁻².

The electrochemical performances of the MoS₂/PANI and MoS₂/PANI/ZnO electrode were measured with cyclic voltammetry. Fig. 7a shows the cyclic voltammetry properties of the synthesized MoS₂/PANI, MoS₂/PANI/ZnO nanocomposites of different concentrations 0.04 M, 0.06 M and 0.08 M of ZnCl₂ at scan rate of 10 mV s⁻¹. The size of the capacitive loop *i.e.* specific capacitance increases with the content of ZnO. This is due to the synergistic effect between the MoS₂/PANI nanocomposites and ZnO nanoparticles [16-18]. Fig. 7b shows the CV curve of the MoS₂/PANI/ZnO nanocomposites of 0.08 M concentration of ZnCl₂ at various scan rates ranging from 10 mV s⁻¹ to 100 mV s⁻¹. It was further observed that the presence of redox peaks attributes to the pseudocapacitive nature of the synthesized nanocomposites. The redox peaks are present even at the high scan rates as observed in the CV diagram. However, a

slight deviation in the shape of CV curve at high scan rate may be due to diffusion of ions into the active material of the electrode [19,20].

Fig. 8a exhibits that the specific capacitance of MoS₂, MoS₂/PANI and MoS₂/PANI/ZnO electrode from 0.04 M to 0.08 M concentration of ZnCl₂ at various scan rate from 10 mV s⁻¹ to 100 mV s⁻¹. The specific capacity of the electrode materials for CV data can be calculated using the following equation [21]:

$$C_s = \frac{1}{mv(V_c - V_a)} \int_{V_a}^{V_c} I dv \quad (1)$$

where C_s is the specific capacitance (F g⁻¹), m is the mass of the prepared nanocomposites (g), v is the scan rate (mV s⁻¹), V_c-V_a is the operative potential (V) and I is the current (A). The calculated specific capacitance of MoS₂/PANI nanocomposites was 323 F g⁻¹ whereas the ZnO doped MoS₂/PANI nanocomposites electrodes show the specific capacitance of 426 F g⁻¹, 462 F g⁻¹ and 536 F g⁻¹ for 0.04 M, 0.06 M and 0.08 M, respectively. The 0.08 M of ZnCl₂ doped electrode have higher active sites and increased surface volume which, results in higher specific capacitance. It is further observed that the specific capacitance decreases with increase in the scan rate. The scan rate directly impacts on the diffusion of H²⁺ ions in the electrodes and at lower scan rates, the electrolyte ions have sufficient time to penetrate pores of the material while at higher scan rates, the ions accumulate on the outer surface. Thus, the capacitance value decreases on increasing the scan rate and this may be due to the limited ion diffusion [21,22]. The EIS spectrum is also recorded for the MoS₂/PANI and MoS₂/PANI/ZnO nanocomposites as shown in Fig. 8b. EIS measurement is executed to study the electrical properties of the 0.08 M of MoS₂/PANI/ZnO nanocomposites. The impedance was measured over the frequency range from 0.01Hz to 100 KHz at an open circuit potential and are displayed in the Nyquist plots. Fig. 8b shows the Nyquist plot of the synthesized material. The imaginary

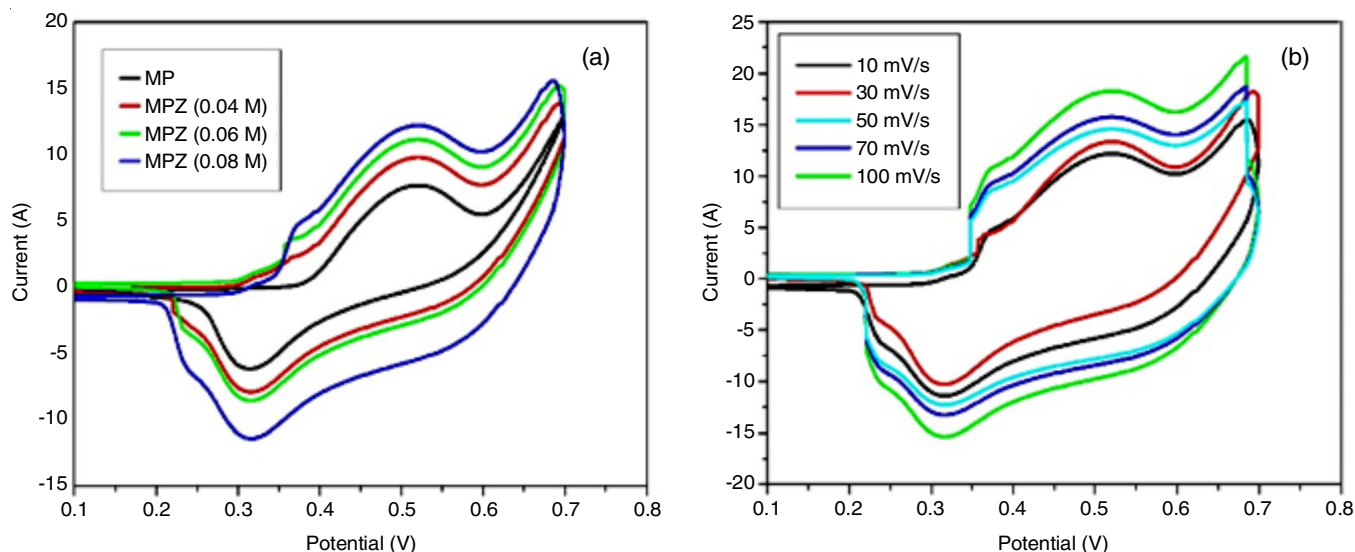


Fig. 7. CV analysis (a) MoS₂/PANI, MoS₂/PANI/ZnO nanocomposites at scan rate 10 mVs⁻¹ using different concentrations of ZnCl₂ from 0.04 M to 0.08 M (b) MoS₂/PANI/ZnO nanocomposites of 0.08 M concentration of ZnCl₂ at various scan rate from 10 mV s⁻¹ to 100 mV s⁻¹

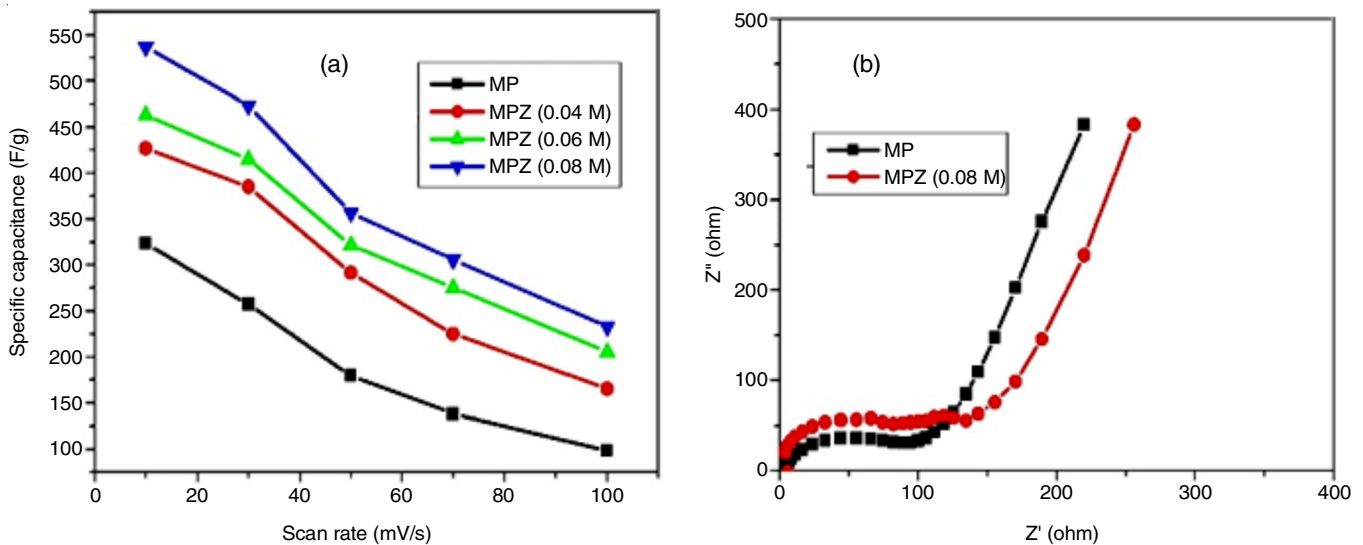


Fig. 8. (a) Specific capacitance of MoS₂/PANI and MoS₂/PANI/ZnO (0.04 M, 0.06 M and 0.08 M) nanocomposites at various scan rate from 10 mV s⁻¹ to 100 mV s⁻¹ using 0.04 M, 0.06 M and 0.08 M concentration of zinc chloride (b) EIS for MoS₂/PANI and MoS₂/PANI/ZnO nanocomposites

component (Z') shows the capacitive properties whereas the real component (Z) shows the ohmic behaviour of the synthesized material, in which the semi-circle behaviour indicates high frequency region and also a sloped linear behavior indicates the low frequency region. A small arc formation in high frequency range emphasizes very low charge transfer that leads to the low resistance and results in high conductivity of the active materials and thereby enhances the energy storage of the material [23].

Fig. 9a shows the galvanostatic charge-discharge curves of the MoS₂/PANI and MoS₂/PANI/ZnO nanocomposites at current density of 0.5 mA cm⁻². The triangular shape of the discharge curve explains the supercapacitor behaviour of the MoS₂/PANI and MoS₂/PANI/ZnO which associates with the CV results. It is observed that the MoS₂/PANI/ZnO of 0.08 M

concentration of ZnCl₂ exhibits the higher specific capacitance. The GCD curves of MoS₂/PANI/ZnO nanocomposites of 0.08 M concentration of ZnCl₂ at different current densities from 0.5 mA cm⁻² to 5 mA cm⁻² is shown in Fig. 9b. The charge-discharge curves show a symmetric shape indicating the 0.08 M of MoS₂/PANI/ZnO electrode have better supercapacitive behaviour and high reversible Faradic reaction between the K⁺ and MoS₂/PANI/ZnO nanocomposites. The increase in the charging time results in high specific capacitance. The specific capacitance can be calculated by the following equation [23,24]:

$$C = \frac{i \times \Delta t}{m} \quad (2)$$

where C (C g⁻¹) is the specific capacity, I (A) is the discharge current, (s) is the discharge time and m (g) is the mass of the electrode material.

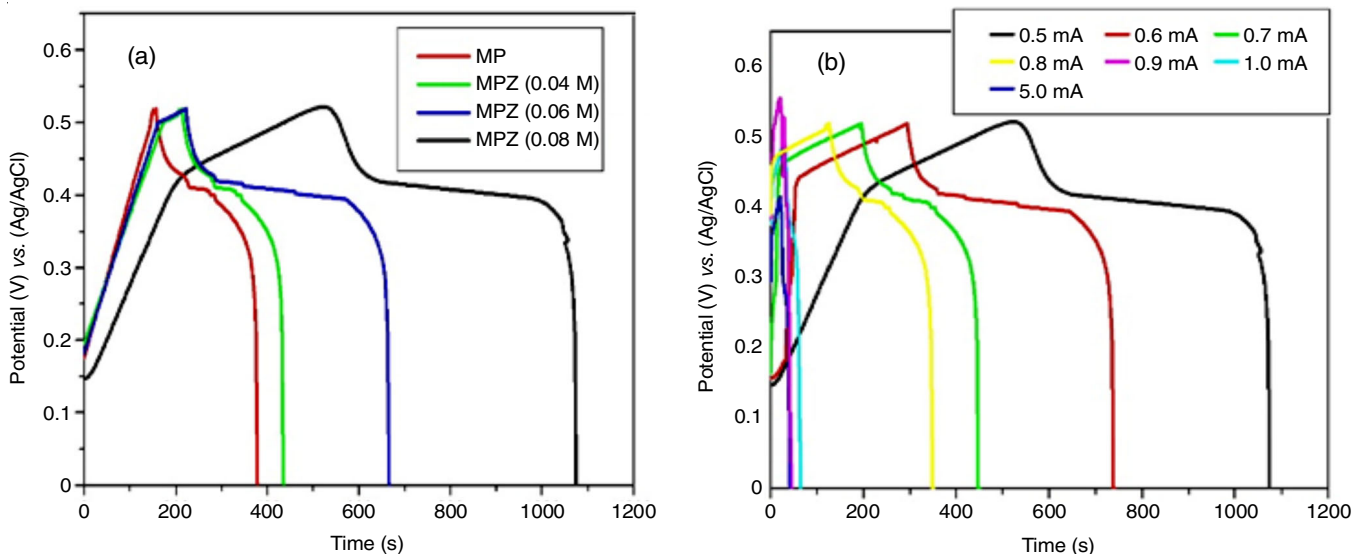


Fig. 9. (a) GCD analysis of MoS₂/PANI nanocomposites, MoS₂/PANI/ZnO nanocomposites from 0.04 M concentration of zinc chloride at current density of 0.5 mA cm⁻² (b) GCD analysis of MoS₂/PANI/ZnO nanocomposites of 0.08 M concentration of zinc chloride at various current density from 0.5 mA cm⁻² to 5.0 mA cm⁻²

Fig. 10a shows the specific capacitance of MoS₂/PANI and MoS₂/PANI/ZnO nanocomposites from 0.04 M to 0.08M concentration of zinc oxide. The specific capacitance values obtained from the GCD curve for MoS₂/PANI was 348 F g⁻¹ whereas, 398 F g⁻¹, 447 F g⁻¹ and 577 F g⁻¹, respectively for 0.04 M, 0.06 M and 0.08 M of ZnCl₂ doped MoS₂/PANI electrodes at current density from 0.5 mA cm⁻². It is observed from the Fig. 10a that the specific capacitance decreases with an increase in the discharge current density because of the occurrence of fast potential changes in the material, which leads to low penetration of the ions into the inner region of pores. The capacitance highly depends on the number of pores in the electrode material. By increasing the concentration, the number of pores in the electrode material increases, which results in higher specific capacitance. The MoS₂/PANI/ZnO nanocomposites with 0.08 M concentration of ZnO exhibits better performance due to the high accessibility of the Faradic reaction. The energy density and power density determine the super capacitive properties of the material and are obtained from charge/discharge. The energy density and power density were calculated by using eqns. 3 and 4, respectively [24]:

Energy density:

$$E = \frac{1}{2}(CV)^2 \quad (3)$$

Power density:

$$P = \frac{E}{t} \quad (4)$$

where *t* is the discharge time obtained from GCD, *C* is the specific capacitance obtained from the GCD and *V* is the operating voltage. It was observed that the power density increases from 74 kW kg⁻¹ to 250 kW kg⁻¹ and the energy density of MoS₂/PANI/ZnO nanocomposites decrease from 60.62 Wh kg⁻¹ to 54.62 Wh kg⁻¹. The electrochemical cycling stability is a crucial factor for the supercapacitor application. Fig. 10b shows the cycling stability test for MoS₂/PANI/ZnO nanocomposites electrode at a current density of 1 mA cm⁻². The specific capaci-

tance slightly decreases with the increase in the cycling number. The MoS₂/PANI/ZnO nanocomposites retain the specific capacitance value even after 5000 cycles. The capacity retention after 5000 cycle was found to be 90%, which thereby confirms the good electrochemical stability.

Conclusion

In this work, MoS₂/PANI/ZnO nanocomposites were synthesized by microwave assisted method. The phase formation and the functional group were confirmed by XRD and FT-IR spectroscopic analysis. The crystallite size of MoS₂/PANI/ZnO nanocomposites of 0.04 M, 0.06 M and 0.08 M concentration of ZnCl₂ were found to be 19 nm, 22 nm and 24 nm, respectively. The FE-SEM and HR-TEM images confirmed the uniform nanosheet stacked with the spherical particles of MoS₂/PANI/ZnO nanocomposites. The UV analysis confirmed the band gap of the MoS₂/PANI/ZnO nanocomposites decrease with the increase in the crystallite size. The electrochemical performances were examined by CV, GCD and EIS techniques. The CV curve shows the presence of redox pair and the EIS (Nyquist plot) confirmed the supercapacitor nature. The GCD analysis revealed the discharge curves and better specific capacitance of 577 F g⁻¹ for MoS₂/PANI/ZnO nanocomposites with 0.08 M concentration of ZnO. The cyclic stability analysis showed the capacitance retention of about 90% after 5000 cycles and thus, the prepared MoS₂/PANI/ZnO nanocomposites were found to be potential electrode material for supercapacitor applications.

CONFLICT OF INTEREST

The authors declare that there is no conflict of interests regarding the publication of this article.

REFERENCES

1. L. Ren, G. Zhang, Z. Yan, L. Kang, H. Xu, F. Shi, Z. Lei and Z.-H. Liu, *ACS Appl. Mater. Interfaces*, **7**, 28294 (2015); <https://doi.org/10.1021/acsami.5b08474>

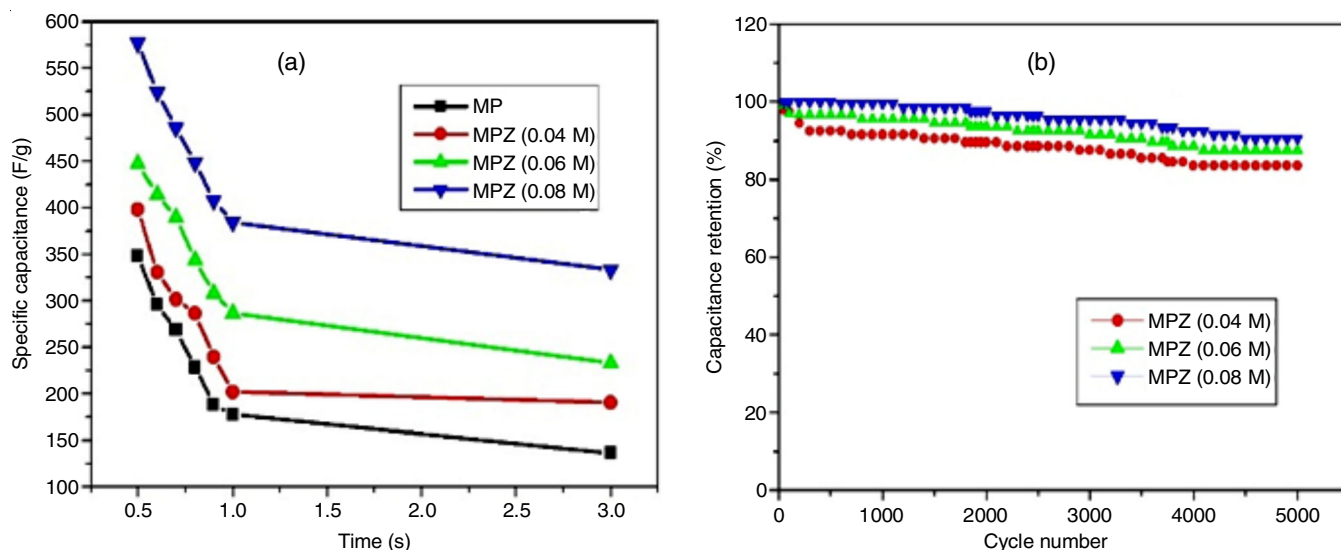


Fig. 10. (a) Specific capacitance of MoS₂/PANI and MoS₂/PANI/ZnO nanocomposites from 0.04 M to 0.08 M concentration of zinc chloride at various current density from 0.5 mA cm⁻² to 3 mA cm⁻² (b) Cyclic stability of MoS₂/PANI/ZnO nanocomposites from 0.04 M 0.06 M and 0.08 M concentration of zinc chloride at current density of 1 mA cm⁻²

2. S.K. Godlaveeti, S. Jangiti, A.R. Somala, H. Maseed and R.R. Nagireddy, *J. Cluster Sci.*, **32**, 703 (2021);
<https://doi.org/10.1007/s10876-020-01833-4>
3. K.-J. Huang, L. Wang, Y.-J. Liu, H.-B. Wang, Y.-M. Liu and L.-L. Wang, *Electrochim. Acta*, **109**, 587 (2013);
<https://doi.org/10.1016/j.electacta.2013.07.168>
4. L.F. Szczepura, J.A. Edwards and D.L. Cedeno, *J. Cluster Sci.*, **20**, 105 (2009);
<https://doi.org/10.1007/s10876-008-0214-5>
5. Z. Gan, X. Lei, B. Hou, M. Luo, S. Zhong and C. Ouyang, *J. Cluster Sci.*, **31**, 643 (2020);
<https://doi.org/10.1007/s10876-019-01736-z>
6. L. Ren, G. Zhang, Z. Yan, L. Kang, H. Xu, F. Shi, Z. Lei and Z.-H. Liu, *ACS Appl. Mater. Interfaces*, **7**, 28294 (2015);
<https://doi.org/10.1021/acsami.5b08474>
7. K.-J. Huang, L. Wang, Y.-J. Liu, H.-B. Wang, Y.-M. Liu and L.-L. Wang, *Electrochim. Acta*, **109**, 587 (2013);
<https://doi.org/10.1016/j.electacta.2013.07.168>
8. S. Dhibar, P. Bhattacharya, G. Hatui, S. Sahoo and C.K. Das, *ACS Sustainable Chem. Eng.*, **2**, 1114 (2014);
<https://doi.org/10.1021/sc5000072>
9. Y. Zhai, Y. Dou, D. Zhao, P.F. Fulvio, R.T. Mayes and S. Dai, *Adv. Mater.*, **23**, 4828 (2011);
<https://doi.org/10.1002/adma.201100984>
10. L. Yu, Q. Wang, H. Yang, Q. Zhang and Z. Luo, *Dalton Trans.*, **46**, 9868 (2017);
<https://doi.org/10.1039/C7DT01170A>
11. K.-J. Huang, J.-Z. Zhang, G.-W. Shi and Y.-M. Liu, *Electrochim. Acta*, **132**, 397 (2014);
<https://doi.org/10.1016/j.electacta.2014.10.079>
12. Zh. A. Boeva and V.G. Sergeev, *Polym. Sci. Ser. C*, **56**, 144 (2014);
<https://doi.org/10.1134/S1811238214010032>
13. S.H. Kazemi M.A. Kiani, R. Mohamadi and L. Eskandarian, *Bull. Mater. Sci.*, **37**, 1001 (2014);
<https://doi.org/10.1007/s12034-014-0037-y>
14. S. Krithika and J. Balavijayalakshmi, *Mater. Res. Express*, **6**, 105023 (2019);
<https://doi.org/10.1088/2053-1591/ab3828>
15. S.B. Kondawar, S.D. Bompilwar, V.S. Khati, S.R. Thakre, V.A. Tabhane and D.K. Burghate, *Arch. Appl. Sci. Res.*, **2**, 247 (2010).
16. A. Mostafaei and A. Zolriasatein, *Prog. Nat. Sci. Mater. Int.*, **22**, 273 (2012);
<https://doi.org/10.1016/j.pnsc.2012.07.002>
17. S. Krithika and J. Balavijayalakshmi, *Mater. Today Proc.*, (2021);
<https://doi.org/10.1016/j.matpr.2021.01.013>
18. P.T. Patil, R.S. Anwane and S.B. Kondawar, *Proced. Mater. Sci.*, **10**, 195 (2015);
<https://doi.org/10.1016/j.mspro.2015.06.041>
19. N. Parveen, S.A. Ansari, M.O. Ansari and M.H. Cho, *J. Colloid Interface Sci.*, **506**, 613 (2017);
<https://doi.org/10.1016/j.jcis.2017.07.087>
20. K. Deb, K. Sarkar, A. Bera, A. Debnath and B. Saha, *Synth. Met.*, **245**, 96 (2018);
<https://doi.org/10.1016/j.synthmet.2018.08.011>
21. B. Saravanakumar, T. Priyadharshini, G. Ravi, V. Ganesh, A. Sakunthala and R. Yuvakkumar, *J. Sol-Gel Sci. Technol.*, **84**, 297 (2017);
<https://doi.org/10.1007/s10971-017-4504-y>
22. J. Zhu, W. Sun, D. Yang, Y. Zhang, H.H. Hoon, H. Zhang and Q. Yan, *Nano. Micro. Small*, **11**, 4123 (2015);
<https://doi.org/10.1002/sml.201403744>
23. O. Koysuren, C. Du, N. Pan and G. Bayram, *J. Appl. Polym. Sci.*, **113**, 1070 (2009);
<https://doi.org/10.1002/app.29924>
24. B. Saravanakumar, S.M. Lakshmi, G. Ravi, V. Ganesh, A. Sakunthala and R. Yuvakkumar, *J. Alloys Compd.*, **723**, 115 (2017);
<https://doi.org/10.1016/j.jallcom.2017.06.249>